[2] L. Alvarez, P. L. Lions, and J. M. Morel, "Image selective smoothing and edge detection by nonlinear diffusion," *SIAM J. Numer. Anal.* vol.29, pp. 845-866, 1992.
[3] S. Angenent, "Parabolic equations for curves on surfaces, Part II. Intersections, blow-up, and generalized solutions," *Annals of Mathematics*, vol. 133, pp. 171–215, 1991.
[4] S. Angenent, G. Sapiro, and A. Tannenbaum, "On the affine heat equation for nonconvex curves," MIT Technical Report – LIDS, April 1994, submitted.
[5] J. Babaud, A. P. Witkin, M. Baudin, and R. O. Duda, "Uniqueness of the Gaussian kernel for scale–space filtering," *IEEE Trans. PAMI*, vol. 8, pp. 26–33, 1986.
[6] W. Blaschke, *Vorlesungen über Differentialgeometrie II*, Verlag Von Julius Springer, Berlin, 1923.
[7] M. Gage, "On an area–preserving evolution equation for plane curves," *Contemporary Mathematics*, vol. 51, pp. 51–62, 1986.
[8] M. Gage and R. S. Hamilton, "The heat equation shrinking convex plane curves," *J. Differential Geometry*, vol. 23, pp. 69–96, 1986.
[9] M. Grayson, "The heat equation shrinks embedded plane curves to round points," *J. Differential Geometry*, vol. 26, pp. 285–314, 1987.
[10] H. W. Guggenheimer, *Differential Geometry*, McGraw–Hill, New York, 1963.
[11] B. K. P. Horn and E. J. Weldon, Jr., "Filtering closed curves," *IEEE Trans. Pattern Anal. Machine Intell.*, vol. 8, pp. 665–668, 1986.
[12] B. B. Kimia, A. Tannenbaum, and S. W. Zucker, "Shapes, shocks, and deformations, I," to appear in *International Journal of Computer Vision*.
[13] J. J. Koenderink, "The structure of images," *Bio. Cyber.*, vol. 50, pp. 363–370, 1984.
[14] D. G. Lowe, "Organization of smooth image curves at multiple scales," *International Journal of Computer Vision*, vol. 3, pp. 119–130, 1989.
[15] F. Mokhtarian and A. Mackworth, "A theory of multi-scale, curvature based shape representation for planar curves," *IEEE Trans. PAMI*, vol. 14, pp. 789–805, 1992.
[16] J. Oliensis, "Local reproducible smoothing without shrinkage," *IEEE Trans. PAMI*, vol. 15, pp. 307–312, 1993.
[17] P. J. Olver, G. Sapiro, and A. Tannenbaum, "Differential invariant signatures and flows in computer vision: A symmetry group approach," MIT Report – LIDS, Dec. 1993. Also in [21].
[18] P. J. Olver, G. Sapiro, and A. Tannenbaum, "Invariant geometric evolutions of surfaces and volumetric smoothing," MIT Report – LIDS, April 1994, to appear in SIAM-JAM.
[19] S. J. Osher, "Volume preserving flows," personal communication, March 1994.
[20] S. J. Osher and J. A. Sethian, "Fronts propagation with curvature dependent speed: Algorithms based on Hamilton–Jacobi formulations," *J. of Comp. Physics*, vol. 79, pp. 12–49, 1988.
[21] B. M. ter Haar Romeny (Ed.), *Geometry Driven Diffusion in Computer Vision*, Kluwer, 1994.
[22] J. Rubinstein and P. Sternberg, "Nonlocal reaction diffusion equations and nucleation," *IMA Journal of Applied Mathematics*, vol. 48 pp. 249–264, 1992.
[23] G. Sapiro, R. Kimmel, D. Shaked, B. B. Kimia, and A. M. Bruckstein, "Implementing continuous–scale morphology via curve evolution," *Pattern Recog.*, vol. 26, no. 9, pp. 1363–1372, 1993.
[24] G. Sapiro and A. Tannenbaum, "On affine plane curve evolution," *Journal of Functional Analysis*, vol. 119, no. 1, pp. 79–120, 1994.
[25] G. Sapiro and A. Tannenbaum, "Affine invariant scale–space," *International Journal of Computer Vision* vol. 11, no. 1, pp. 25–44, 1993.
[26] G. Sapiro and A. Tannenbaum, "Image smoothing based on an affine invariant flow," *Proc. of Conf. on Info. Sciences and Sys.*, Johns Hopkins University, March 1993.
[27] G. Sapiro and A. Tannenbaum, "On invariant curve evolution and image analysis," *Indiana University Mathematics Journal*, vol. 42, no. 3, pp. 985–1010, 1993.
[28] G. Sapiro and A. Tannenbaum, "Area and Length Preserving Geometric Invariant Scale–Spaces," MIT Report – LIDS–2200, September 1994.
[29] A. P. Witkin, "Scale–space filtering," *Int. Joint. Conf. Art. Intell.*, pp. 1019–1021, 1983.
[30] A. L. Yuille and T. A. Poggio, "Scaling theorems for zero crossings," *IEEE Trans. PAMI* vol. 8, pp. 15–25, 1986.

Texture Segmentation Using Fractal Dimension

B. B. Chaudhuri and Nirupam Sarkar

***Abstract*—This paper deals with the problem of recognizing and segmenting textures in images. For this purpose we employ a technique based on the fractal dimension (FD) and the multi–fractal concept. Six FD features are based on the original image, the above average/high gray level image, the below average/low gray level image, the horizontally smoothed image, the vertically smoothed image, and the multi–fractal dimension of order two. A modified box–counting approach is proposed to estimate the FD, in combination with feature smoothing in order to reduce spurious regions. To segment a scene into the desired number of classes, an unsupervised *K*–means like clustering approach is used. Mosaics of various natural textures from the Brodatz album as well as microphotographs of thin sections of natural rocks are considered, and the segmentation results to show the efficiency of the technique. Supervised techniques such as minimum–distance and *k*–nearest neighbor classification are also considered. The results are compared with other techniques.**

***Index Items*—Texture, segmentation, fractal dimension, multi–fractal, classification.**

I. Introduction

There are two important aspects of texture image segmentation procedures, namely *feature extraction* and *segmentation*. Examples of commonly used texture features are: Fourier transform energy [1], local extrema [2], co–occurrence statistics [3], [4], dominant local orientation and frequency [5], directional gray–level energy [6], [7], directional filter masks including Gabor filters [8], [9], [10], finite prolate spheroidal sequences [11] as well as fractal dimension [12], [13]. Features derived from the autoregressive moving average model [14], the Gaussian–Markov random field model [15], and the Gibbs random field model [16] are also used. Segmentation methods, on the other hand, are based on region growing [1], [2], estimation theory [15], split–and–merge [3], Bayesian classification [7], relaxation [7], clustering [13], [17], and neural networks [8], [9].

The texture features studied here are all based on the fractal geometry of images. This choice is motivated by the observation that the fractal dimension (FD) is relatively insensitive to an image scaling [18], and shows a strong correlation with human judgment of surface roughness. Field [19] has shown that many natural textures have a linear log power spectrum, and that the processing in the human visual system (i.e. the Gabor–type representation) is well suited to characterize such textures. A linear log power spectrum is related to the fractal dimension, but it is an idealization for many textures. In this sense, the fractal dimension is an approximative spectral estimation and comparable to alternative methods [10].

The texture segmentation in this article is based on six FD–based features. To this purpose, a modified box–counting method is used for estimating the FD [20]. The so–called differential box counting method, described in Sec. 2, is faster and more accurate than other

Manuscript received Sept. 13, 1993; Revised April 13, 1994. Recommended for acceptance by Dr. Anil K. Jain.
B. B. Chaudhuri is a senior member of the IEEE.
IEEE Log Number P95002

box–counting approaches [21], [22], [12]. The features are defined in Sec. 3, and the smoothing and segmentation approaches are treated in Sec. 4. The methods are tested on various combinations of digitized textures from the Brodatz album [23] and microphotographs of thin sections of natural rocks. The experimental results are presented in Sec. 5.

II. Fractal Dimension Estimation

The Hausdorff–Besicovitch(HB) or fractal dimension of a bounded set A in $I\!R^n$ is a real number used to characterize the geometrical complexity of A. A set is called a fractal set if its HB dimension is strictly greater than its topological dimension. Mandelbrot [24] coined the term fractal from the Latin word *fractus*, which means irregular segments.

The concept of self–similarity can be used to estimate the fractal dimension. A bounded set A in Euclidean n–space is self–similar if A is the union of N_r distinct (non–overlapping) copies of itself scaled up or down by a ratio r. The fractal dimension D of A is given by the relation [24]:

$$1 = N_r r^D \quad \text{or} \quad D = \frac{\log(N_r)}{\log(1/r)} \tag{1}$$

There exist several approaches to estimate the FD of an image [25], [18], [22], [12]. These methods are either computationally expensive or cover only a small part of the dynamic range of FD. A method, called the Differential Box Counting (DBC) method [20], that covers a wide dynamic range is used here.

Equation (1) is the basis of estimating the FD by the DBC approach. Here, N_r is determined in the following way. Assume that the image of size $M \times M$ pixels has been scaled down to a size $s \times s$ where $M/2 \geq s > 1$ and s is an integer. Then we know that $r = s/M$. Now, consider the image as a 3D space with (x, y) denoting 2D position and the third coordinate (z) denoting gray–level. The (x, y) space is partitioned into grids of size $s \times s$. On each grid there is a column of boxes of size $s \times s \times s$. Let the minimum and maximum gray level of the image in the $(i, j)^{th}$ grid fall in the k^{th} and the l^{th} box, respectively. Then

$$n_{r(i,j)} = l - k + 1 \tag{2}$$

is the contribution of N_r in the $(i, j)^{th}$ grid. Taking contributions from all grids, we have

$$N_r = \sum_{i,j} n_r(i, j). \tag{3}$$

N_r is counted for different values of r (*i.e.* different values of s). Then using (1) we can estimate D, the fractal dimension, from the least–squares linear fit of $\log(N_r)$ against $\log(1/r)$. Because of the differential nature of $n_r(i, j)$ we call this the Differential Box Counting (DBC) method. In the actual implementation, a random placement of boxes is applied in order to reduce quantization effects.

The success of the DBC method is attributed to the fact that differential box counting by equations (2–3) gives a better approximation to the boxes intersecting the image intensity surface relative to other box counting methods. In a sense, it is an approximation to the blanket method [25]. Comparative results with DBC and other methods are described in [20].

III. Feature Selection

Mandelbrot and Van Ness [26] and Voss [21] have pointed out that different textures may have the same FD. This may be due to combined differences in coarseness and directionality (dominant orientation and degree of anisotropy). We propose to use six features in order to discriminate these aspects. They are based on the FD of: (1) the original image, (2) the high gray–valued image, (3) the low gray–valued image, (4) the horizontally smoothed image, (5) the vertically smoothed image and (6) the multi–fractal dimension of the original image. For any feature f, we have $f \in [0,1]$.

Feature 1. The FD of the original image I_1 is computed on overlapping windows of size $(2W + 1) \times (2W + 1)$. Thus, at point (i, j) the first feature value $F_1(i, j)$ is defined as

$$F_1(i, j) = FD\{\ I_1(i+l, j+k);\ \ -W \leq l, k \leq W\ \}, \tag{4}$$

where FD is the fractal dimension derived by the method described in Sec. 2. Since $2.0 < F_1(i, j) \leq 3.0$, we define the normalized feature as $f_1(i, j) = F_1(i, j) - 2$ so that $0 \leq f_1(i, j) \leq 1$.

Features 2–3. Consider two modified images called high and low gray–valued images I_2 and I_3 respectively, defined as

$$I_2(i, j) = \begin{cases} I_1(i, j) - L_1 & \text{if } I_1(i, j) > L_1 \\ 0 & \text{otherwise} \end{cases} \tag{5}$$

$$I_3(i, j) = \begin{cases} 255 - L_2 & \text{if } I_1(i, j) > (255 - L_2) \\ I_1(i, j) & \text{otherwise} \end{cases} \tag{6}$$

$L_1 = g_{min} + av/2$; $L_2 = g_{max} - av/2$ while g_{max}, g_{min} and av denote the maximum, minimum and average gray value in I_1, respectively. If two images I_1 and J_1 have a same FD, their high gray–valued images I_2 and J_2 may not have an identical roughness and their FDs would be different. The same holds for I_3 and J_3. The normalized features f_2 and f_3 are computed from I_2 and I_3 similar to the computation of f_1 from I_1.

Features 4–5 The FD of an image is related to its roughness and hence it is reduced by gray value smoothing. For a highly oriented texture, the FD will be affected least if the texture is smoothed along the direction of its dominant orientation. But if the smoothing direction is perpendicular, the FD will be substantially reduced. On the other hand, a texture having a low degree of anisotropy will show an identical effect on the FD irrespective of the smoothing direction.

We take images smoothed in the horizontal or vertical direction and compute their FD as the fourth and fifth feature. Horizontally and vertically smoothed versions of the image are defined as

$$I_4(i, j) = \frac{1}{2w+1} \sum_{k=-w}^{w} I(i, j+k) \tag{7}$$

$$I_5(i, j) = \frac{1}{2w+1} \sum_{k=-w}^{w} I(i+k, j) \tag{8}$$

The normalized FD features f_4 and f_5 are computed similar to f_1.

Feature 6. The FD measures defined above can only characterize

self–similarity in ideal cases. Most real textures are not ideal fractals. For a self–similar distribution showing anisotropic and inhomogeneous scaling properties, the multi–fractal concept is a better approach [27], because it implies a continuous spectrum of exponents for the pattern characterization. Our sixth feature is based on the multi–fractal with exponent of order two. Following Pietronero [27] we describe briefly the basic concept of multi–fractals.

The pointwise dimension (or singularity exponent) α is defined as

$$\lim_{r\to 0} \mu_r(x) \sim r^{\alpha} \tag{9}$$

where $\mu_r(x)$ is the distribution in a sphere of radius r around the point x.

In practice we take again $r = s/M$. Hence the distribution at the $(i, j)^{th}$ position is $\mu_r(i, j) = n_r(i, j)/N_r$ where $n_r(i, j)$ and N_r are defined by equation (2) in Sec. 2. We define the partition function $\chi(q,r)$ as follows :

$$\chi(q,r) = \sum_{i,j} \left[\mu_r(i,j)\right]^q \sim r^{\tau(q)}$$

The role of this function is to evaluate all possible singularities of the distribution by studying all the q moments. The exponent $\tau(q)$ defines the small r behavior of $\chi(q,r)$.

From the point of view of the generalized FD $D(q)$, we have

$$(q-1)D(q) = \tau(q) = \lim_{r\to 0} \frac{\ln \chi(q,r)}{\ln r} \quad , \; q \neq 1$$

Our normalized sixth feature f_6 is defined

$$f_6 = TD - D(2) \tag{10}$$

where TD is the topological dimension, which is 2 in this case.

IV. Feature smoothing and Segmentation

If the features are directly used for segmentation, considerable misclassification may occur in the inner regions and at region boundaries. Feature smoothing can reduce the misclassification inside texture regions. Normal moving window averaging results in considerable blurring at the boundaries and therefore an edge–preserving smoothing technique [7] should be used. For our purpose we use the Edge Preserving Noise Smoothing Quadrant (EPNSQ) filtering approach [7]. Consider four quadrants within a $(2w+1) \times (2w+1)$ neighborhood around the center at (i, j), as shown in Fig. 1.

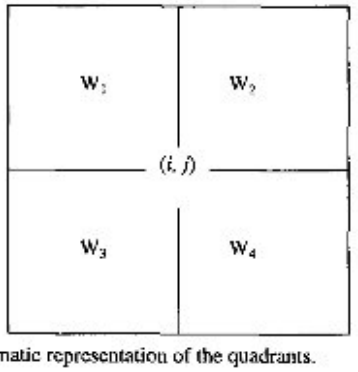

Fig. 1. Schematic representation of the quadrants.

The m^{th} feature value average and variance are computed on each window

$$A_{m,W_n}(i,j) = \frac{1}{w^2} \sum_{k,l \in W_n} f_m\left(i + (-1)^{\lfloor (n+1)/2 \rfloor} k, j + (-1)^n l\right), \tag{11}$$

$$V_{m,W_n}(i,j) = \frac{1}{w^2} \sum_{k,l \in W_n} \left[f_m\left(i + (-1)^{\lfloor (n+1)/2 \rfloor} k, j + (-1)^n l\right) - A_{m,W_n}(i,j) \right]^2 \tag{12}$$

where $A_{m,Wn}(i, j)$ and $V_{m,Wn}(i, j)$; $n = 1,...,4$ represent the average and variance computed on the quadrants W_n around (i, j).

According to the EPNSQ approach the feature value at (i, j) is replaced by $A_{m,Wn}(i, j)$ for which the measured variance $A_{m,Wn}(i, j)$ is minimum.

The segmentation is essentially based on a K–means clustering approach. It is known that the results of the K–means algorithm depends on the choice of cluster seed points. A histogram–based approach of cluster seed point selection is used here. For the i^{th} feature f_i, let H_i be the histogram. Find the dominant peaks of the histogram. Let N_i denote the number of dominant peaks in H_i and let the peaks occur at $f_{i1}, f_{i2},\ldots\ldots, f_{iN_i}$. An average non–overlapping span(S_i) of the i^{th} feature is calculated as $(f_{iN_i} - f_{i1})/(2N_i)$. The cut–off span (S_c) and the average radius (R) of a cluster in the feature space are defined as

$$S_c = \sqrt{\sum_{i=1}^{6} S_i^2} \quad ; \quad R = \sqrt{\frac{A}{\pi \times K}}$$

where A is area of the feature image and K is the number of clusters.

The feature vector of the point at the location (0,0) in the feature image is chosen as the first initial cluster. All the remaining points are scanned one by one. The scanned point p is considered to be a seed point if (i) the Euclidean distance between the feature vector of the scanned point p and each of the other chosen clusters exceeds S_c and (ii) if p is at a distance greater than R from the position of any other chosen points.

This process is continued until all the points are considered. In this way we obtain $K_0 > K$ seed points. Each seed point generates a separate cluster. These K_0 clusters are then iteratively reduced to K clusters by redistributing the data of smallest cluster among the other clusters. Once the K clusters have been obtained, the K–means algorithm [28] is run to get the final clustering. The result, when mapped from feature space to image space, yields the texture segmentation.

V. Experimental Results and Discussion

To test the performance of the set of fractal dimension features, different images were constructed using Brodatz album textures [23]. First, we took six mosaics of four textures, each mosaic of size 256×256 pixels with a dynamic range of 256 gray levels. The six FD features were computed at each pixel (i, j) using a moving window of size 17×17 pixels around (i, j). The feature smoothing was done using a window of size 7×7. The unsupervised approach based on minimum–distance and k–nearest neighbor classification [28] were tested on these smoothed features. The number of training samples used to compute the centroid for a minimum distance classification was 50. In the k–nearest neighbor technique, the chosen values of k are 1 and 5 whereas the number of training samples were 25 and 50. The classification results are presented in Table I. From Table I it can be seen that the methods give roughly identical classification accuracies on these mosaics. Also, we tested the unsupervised

TABLE I
COMPARISON OF DIFFERENT CLASSIFICATION APPROACHES

Plate Number	Texture Mosaic		Unsupervised technique	1NN		5NN		Min-dist
				A	B	A	B	
1	D04	D33	94.93	87.00	87.00	85.81	86.90	85.28
	D68	D28						
2	D77	D84	96.83	96.60	96.66	96.62	96.95	96.97
	D55	D65						
3	D17	D55	97.00	96.89	96.67	97.05	96.68	97.10
	D77	D92						
4	D24	D68	95.40	94.68	94.68	94.65	94.72	94.68
	D03	D77						
5	D04	D09	91.11	92.55	92.55	91.60	92.26	91.40
	D28	D54						
6	D04	D09	91.63	90.76	91.00	90.38	90.46	90.39
	D28	D24						
Average			94.49	93.08	93.09	92.70	93.00	92.62

A - taking 25 training samples, B - taking 50 training samples

approach on the synthetic four–texture mosaic generated by a Gaussian Markov random field model [29]. See Fig 2(a–b), where 96.3 percent correct classification was achieved.

To see the effect of increasing the number of textures, we considered also mosaics of 5, 6, 9 and 16 textures. Using the unsupervised approach, the classification accuracies for 5, 6, 9 and 16 texture mosaics were 95.82 percent, 94.41 percent, 93.7 percent, and 91 percent, respectively. The segmentation result of the 16 texture mosaic in Fig. 3(a) is shown in Fig. 3(b).

Keller *et al* [12] considered texture mosaics similar to ours. Their segmentation approach is also based on the FD of the original image and a "lacunarity" measure. We were inspired by the work in [12]. However, a comparative study [30] of different methods showed that the FD alone performs poorly in texture segmentation. So we used several FD-based features, along with feature domain smoothing and clustering to obtain excellent segmentation.

Fig. 2(a). Four texture mosaic generated by Gaussian Markov random field model.

Among other methods Hsiao and Sawchuk [7] used Law's [6] texture energy as a feature. They used Bayesian classification and reported 95 percent, 93 percent, and 88 percent accuracy for mosaics of 4, 5, and 8 textures.

Jain and Farrokhnia [8] and Farrokhnia [9] used a Gabor filter bank for texture feature extraction. Their classifier was based on a feed–forward neural network model, among other techniques. For a synthetic four–texture mosaic generated by a Gaussian Markov random field model, an accuracy of nearly 97 percent was reported. For a mosaic of 5 textures 94 percent and 96 percent correct classifications were achieved using 10 and 100 training cycles in neural net, respectively. For a mosaic of 16 textures an accuracy of 87 percent and 92.5 percent using 10 and 100 training cycles, respectively, were obtained.

Fig. 2(b). Segmentation mapping of 2(a).

To examine the efficiency of the segmentation approach for more complex situations, photographs of natural rocks were taken. Fig. 4(a) shows one of the microphotographs of a thin (of thickness

< 0.03 mm) rock section of sandstone at a magnification of 160 ×, taken with episcopic illumination. Its constituents are fine grained quartz particles and iron cementing materials. The problem is to separate the two types of materials by texture segmentation approach. The segmentation result is shown in Fig. 4(b) where the black region is cement and the white region is quartz. It was compared with human expert judgment and they agreed in 91.7 percent by area match.

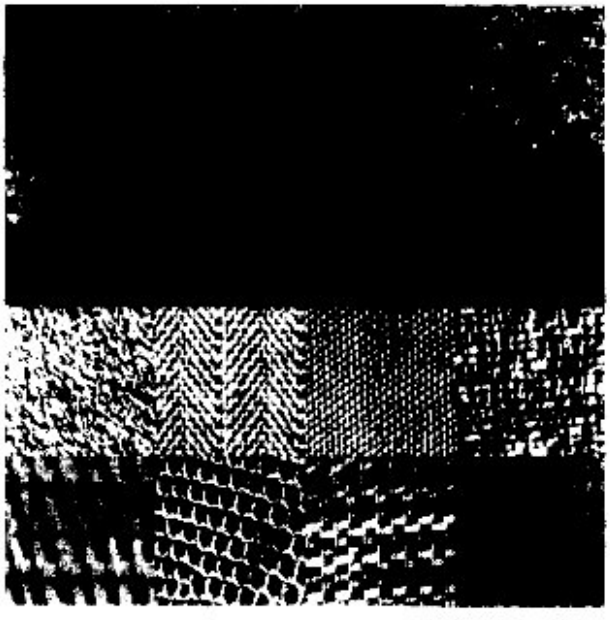

Fig. 3(a). Texture mosaic of sixteen natural textures (D06, D05, D82, D92; D54, D21, D20, D34; D04, D17, D77, D84; D65, D03, D55, D101).

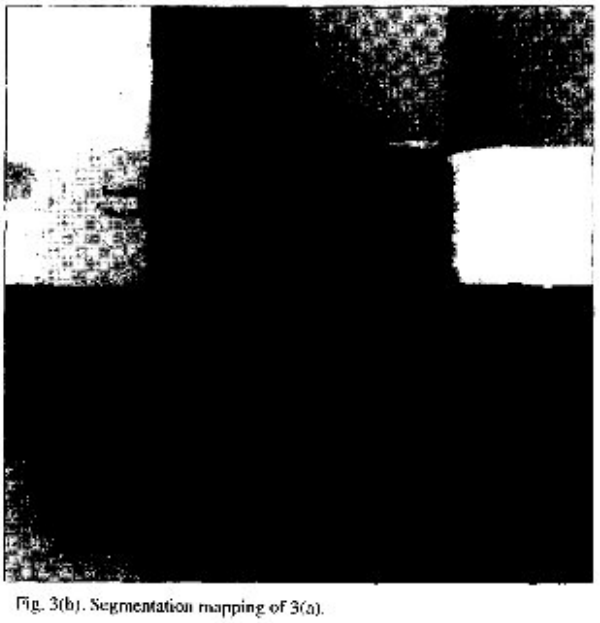

Fig. 3(b). Segmentation mapping of 3(a).

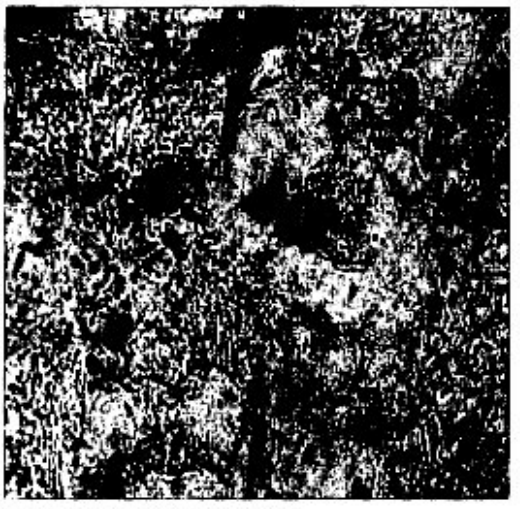

Fig. 4(a). Coarse grain cemented sandstone.

Fig. 4(b). Segmentation mapping of 4(a).

ACKNOWLEDGMENT

The authors wish to thank Prof. A. K. Jain for supplying some of the texture images from the Brodatz album.

REFERENCES

[1] R. Bajcsy, "Computer identification of visual surfaces", *Computer Graphics and Image Processing*, vol. 2, pp. 118–130, 1973.

[2] S. G. Carlton and O. R. Mitchell, Image segmentation using texture and gray level, *Proc. IEEE Conf. Pattern Recog. Image Processing*, 1977.

[3] T. Pavlidis and P. C. Chen, "Segmentation by texture using co–occurence matrix and split–and–merge algorithm," *Computer Graphics and Image Processing*, vol. 10, pp. 172–182, 1979.

[4] R. W. Conners, M. M. Trivedi and C. A. Harlow, "Segmentation of a high resolution urban scene using texture operators," *Computer Vision Graphics and Image Processing*, vol. 25, pp. 273–310, 1984.

[5] H. Knutsson and G. H. Granlund, "Texture analysis using two dimensional quadratic filter," *ICASSP 83, IEEE Conf. on Acoustics, Speech and Signal Process*, 1983.

[6] K. I. Laws, "Rapid texture identification," *SPIE*, vol. 238, pp. 376–380, 1980.
[7] J. Y. Hsiao and A. A. Sawchuk, "Supervised Textured Image Segmentation Using Feature Smoothing and Probabilistic Relaxation Techniques," *IEEE Trans on Pattern Anal. and Machine. Intell.*, vol. 11, pp. 1279–1292, 1989.
[8] A.K. Jain and F. Farrokhnia, "Unsupervised texture segmentation using gabor filters," *Pattern Recognition*, vol. 24, pp. 1167–1186, 1991.
[9] F. Farrokhnia, "Multi–channel filtering techniques for texture segmentation and surface quality inspection," Ph.D. Thesis, Michigan State Univ., 1992.
[10] J. M. H. Du Buf, "Abstract processes in texture discrimination," *Spatial Vision*, vol., 6 , 1992.
[11] R. Wilson and M. Spann, "Finite prolate spheroidal sequences and their application ii: Image feature description and segmentation," *IEEE Trans. on Pattern Anal. and Machine Intell.*, vol. 10, pp. 193–203, 1988.
[12] J. Keller, R. Crownover and S. Chen, "Texture Description and Segmentation through Fractal Geometry," *Computer Vision Graphics and Image Processing*, vol. 45, pp. 150–160, 1989.
[13] B. B. Chaudhuri, N. Sarkar and P. Kundu, "An Improved Fractal Geometry Based Texture Segmentation Technique", *Proc. IEE–part E*, pp. 140. 223–241, 1993.
[14] C. W. Therrien, "An estimation–theoretic approach to terrain image segmentation", *Computer Vision, Graphics and Image Processing*, vol. 22, pp. 313–326, 1983.
[15] S. Chatterjee and R. Chellappa, "Maximum likelihood texture segmentation using Gaussian Markov random field models," *Proc. IEEE Conf Computer Vision. Graph, Pattern Recog.*, 1985.
[16] H. Derin and H. Elliot, "Modelling and segmentation of noisy and textured images using Gibbs random fields", *IEEE Trans on Pattern Anal. and Machine. Intell.* vol. 9, pp. 39–55, 1987.
[17] M. Spann and R. Wilson, "A quad–tree approach to image segmentation which combines statistical and spatial information, *Pattern Recognition*. vol. 18, pp. 257–269, 1985.
[18] A. P. Pentland, "Fractal based description of natural scenes," *IEEE Trans. on Pattern Anal. and Machine Intell*, vol. 6, pp. 661–674, 1984.
[19] D. J. Field, "Relations between the statistics of natural images and the response properties of cortical cells," *Journal Optical Society America*, vol. A4, pp. 2379–2394, 1987.
[20] N. Sarkar and B.B. Chaudhuri, "An efficient approach to estimate fractal dimension of texture image," *Pattern Recognition*, vol. 25, pp. 1035–1041, 1992.
[21] R. Voss, "Random fractals: characterization and measurement," *Scaling Phenomena in Disordered Systems*, R.Pynn and A. Skjeltorp, eds., Plenum, New York, 1986.
[22] J.J. Gangepain and C. Roques–Carmes, "Fractal approach to two dimensional and three dimensional surface roughness," *Wear*, vol. 109, pp. 119–126, 1986.
[23] P. Brodatz, *Textures: A Photographic Album for Artists and Designers*, Dover, New York1966.
[24] B. B. Mandelbrot, *Fractal Geometry of Nature*, Freeman Press, San Francisco, 1982.
[25] S. Peleg, J. Naor, R. Hartley and D. Avnir, "Multiple resolution texture analysis and classification," *IEEE Trans. on Pattern Anal. and Machine Intell*, vol. 6, pp. 518–523, 1984.
[26] B. B. Mandelbrot and J. Van Ness, "Fractional Brownian motion, fractional noise and applications," *SIAM Review*, vol. 10, 1968.
[27] L. Pietronero and R. Kupers, "Fractals in physics," L. Pietronero and E. Tosatti, eds., North–Holland, Amsterdam, 1986.
[28] J. T. Tou and R. C. Gonzalez, *Pattern Recognition Principles*, Addison–Wesley, Reading, MA, 1982.
[29] R. Chellappa, S. Chatterjee and R. Bagdazian, "Texture synthesis and compression using Gaussian random field model," *IEEE Trans. on System, Man and Cybernetics*, vol. 15, pp. 298–303, 1985.
[30] J. M. H. Du Buf, M. Kardan and M. Spann, "Texture feature performance for image segmentation," *Pattern Recognition*, vol. 23, pp. 291–309, 1990.

Fundamental Limitations on Projective Invariants of Planar Curves

Kalle Åström

***Abstract*—In this paper, some fundamental limitations of projective invariants of non-algebraic planar curves are discussed. It is shown that all curves within a large class can be mapped arbitrarily close to a circle by projective transformations. It is also shown that arbitrarily close to each of a finite number of closed planar curves there is one member of a set of projectively equivalent curves. Thus a continuous projective invariant on closed curves is constant. This also limits the possibility of finding so called projective normalisation schemes for closed planar curves.**

***Index Items*— Projective and affine invariants, recognition, Hausdorff metric.**

I. Introduction

The pinhole camera is often an adequate model for projecting points in three dimensions onto a plane. Using this model it is straightforward to predict the image of a collection of objects in specified positions. The inverse problems, to identify and to determine the three-dimensional positions of possible objects from an image, are however much more difficult. Traditionally recognition has been done by matching each model in a model data base with parts of the image. Recently, model based recognition using viewpoint invariant features of planar curves and point configurations has attracted much attention, [7]. Invariant features are computed directly from the image and used as indices in a model data base. This gives algorithms which are significantly faster than the traditional methods. These techniques cannot, however, be used to recognise general curves or point features in three dimensions by means of one single image. Additional information, e.g. that the object is planar, is needed. For point configurations the reason is that only trivial invariants exist in the general case, as is shown in [4], [9]. In this paper it is shown that there are some fundamental limitations also for planar curves.

More specifically, two theorems are presented that elucidate these limitations. The first one, in Section II, states that each curve in a large class can be transformed into a curve arbitrarily close to a circle in a strengthened Hausdorff metric. The second theorem, in Section III, states that given a finite number of closed planar curves $\Gamma_1, \ldots, \Gamma_m$, it is possible to construct a set of *projectively equivalent* planar curves $\Gamma'_1, \ldots, \Gamma'_m$, such that Γ'_i in the Hausdorff metric is arbitrarily close to Γ_i, $i=1, \ldots, m$. These two theorems enlighten the limitations of invariant based recognition schemes. The first one tells us that choosing a distinguished frame by maximising some feature over all projective transformations is not suitable, since in the limit many curves look like circles. The second theorem tells us more generally that every continuous invariant must be constant. Some consequences of these theorems will be discussed in Section IV. Their relevance to computer vision is that the euclidean errors in image processing do not interact well with projective equivalence.

Manuscript received Sept. 27, 1993; Revised June 6, 1994. Recommended for acceptance by Dr. Ruud Bolle.

Kalle Åström is at the Dept. of Mathematics at Lund University, Box 118, S-221 00 Lund, Sweden. The work has been supported by the Swedish National Board for Technical and Industrial Development (NUTEK). The work is done within the ESPRIT–BRA project View-point Invariant Visual Acquisition.

IEEE Log Number P95003